Anal. Bioanal. Electrochem., Vol. 12, No. 6, 2020, 747-765

Analytical & Bioanalytical Electrochemistry

2020 by CEE
www.abechem.com

Full paper

Effect of Procedure Time on Microstructure and Corrosion Behavior of $ZrTiO_4/ZrO_2$ Nanocomposite Coatings by Plasma Electrolytic Oxidation (PEO) Applied on the Ti-6Al-4V Substrate

Elham Nikoomanzari, Kazem Babaei and Arash Fattah-alhosseini*

Department of Materials Engineering, Bu-Ali Sina University, Hamedan 65178-38695, Iran

*Corresponding Author, Tel.: +988138292505; Fax: +988138257400

E-Mail: a.fattah@basu.ac.ir

Received: 6 May 2020 / Received in revised form: 26 May 2020 / Accepted: 6 June 2020 / Published online: 30 June 2020

Abstract- In this research, the effect of PEO procedure time on the distinct properties of coatings such as morphology, chemical composition, roughness and corrosion has been studied. A scanning electron microscopy equipped with an energy dispersive spectroscopy was used to study the microstructure of the coatings. In addition, x-ray diffraction (XRD) and roughness meter were used to evaluate the chemical composition and roughness of the coatings, respectively. The corrosion properties of coatings have been also studied by polarization and electrochemical impedance experiments in the Hank's physiological solution. The results of microstructural analysis showed that rising the time of the coating procedure resulted in an increase in the size of porosity, thickness and roughness. The results of the XRD pattern showed that all coatings were composed of two phases of zirconia and zirconium titanate and that the change in time of coating did not alter the chemical composition of the coating. In the case of corrosion resistance of coatings, the most corrosion potential (611 mV) with the least corrosion current density (18.50 nA/cm^2) in the coating created at the end of the third step of coating (10 minutes) resulted in the most corrosion resistance (0.602 $M\Omega.cm^2$).

Keywords- Ti-6Al-4V substrate; Plasma electrolytic oxidation (PEO); ZrO_2 nanoparticles; Corrosion behavior; Hank's physiological solution

1. INTRODUCTION

One of the most appropriate options to produce orthopedic and dental implants is titanium and its alloys [1–3]. Among titanium and its alloys, the proportion Ti-6Al-4V alloy in producing commercial medical devices is about 20 to 30 percent [4]. Features like low density, high ratio of strength to weight, mechanical properties and proper corrosion behavior have resulted in its potential usage in the field of biomedical [5,6]. The accumulation of abrasive particles around the implant can cause serious problems such as implantation loosening and inflammation and infection around the implant due to unpleasant tribological properties as well as the release of Al and V ions and their entrance into the bloodstream [7–11]. Coating techniques can be utilized in order to solve these problems. Appropriate coating techniques not only preserve the properties of bulk titanium and its alloys including fatigue strength and elastic modulus, but also give it specific surface properties for diverse usages [12].

One of the most highly utilized coating method is PEO that aims at obtaining characteristics like increasing corrosion resistance, improving abrasion behavior, improving fatigue mechanism, biocompatibility, creating stability and faster stabilization of implant in the bone, reducing release of metal ions and improving cell growth have been applied on titanium and its alloys [13–20]. The PEO procedure is a customary electrochemical method in which the inherent oxide of the substrate thickens due to the application of voltage to the immersed substrate in the electrolyte [21,22]. As the thickness of the oxide layer increases, the voltage increases rapidly and when the voltage reaches the breaking potential, the dielectric failure of the oxide layer occurs [23–27]. As a result of dielectric failure, visible sparks will appear on the surface of background. The PEO procedure produces coatings having a two-layer structure [28–30].

In the PEO procedure, the used electrolyte, additives, coating time and electrical parameters, the distance between the anode and the cathode, the speed of electrolyte stirring play major roles in specifying the properties of the two-layer PEO coating [31,32]. Widespread investigations have been done on optimizing the parameters affecting the PEO process in order to improve the different properties of the coating for various applications So far. One of the significant efforts in this field is to modify the electrolyte composition by nanoparticles or micro-grains addition to create composite coatings having appropriate properties [33]. The procedure of particle absorption occurs under high temperature and discharge pressure and the nature of the particle can lonely specify the mode of particles entrance into the coating. The ways that particles can enter the coating are inert or reactive.

The way particles enter depends on the used electrical parameters, the electrolyte chemical composition and the properties of the particles like size, melting point, and chemical stability. Inactive entrance occurs when particles enter the coating with no reaction and producing a new phase. Reactive input also occurs when particles are melted by high-

energy discharges and then react again with components within the electrolyte and substrate [34,35].

In our previous investigation [36], the effect of zirconia nanoparticle concentration on chemical composition, corrosion behavior and antibacterial properties was studied. The results of XRD pattern exhibited that zirconia nanoparticles were in the form of inert and reactive and made ZrO_2 and $ZrTiO_4$ phases, respectively. The results of the corrosion test also indicated that the specimen with 3 g/l of zirconia nanoparticles had the best corrosion behavior and further increasing the concentration of nanoparticles augmented surface discontinuity and declined corrosion resistance. Zirconium titanate is a great ceramic for optical, catalytic, electronic and biomedical applications due to its properties like proper corrosion resistance and abrasion as well as excellent thermal and electrical properties. Furthermore, zirconia desirable properties including great mechanical strength, good corrosion resistance, biocompatibility, chemical stability have resulted in its use in the field of implants, particularly orthopedic and dental implants [37–40]. Li et al. [41] studied the tribological properties of composite coatings having phases of zirconium titanate and zirconia that were created by adding various concentrations of zirconia microparticles to the electrolyte. They reported that the existence of phases of zirconia and zirconium titanate in the coating amended abrasion behavior, and specimens with 3 and 6 g/l zirconia indicated the highest abrasion resistance since further increase in zirconia concentration raised the roughness of surface and as a result decreased the wear resistance [41].

The coating procedure time is one of the effective parameters in the coating properties, particularly the corrosion, abrasion, mechanical and photocatalytic properties of the coating [42–44]. Cheng et al. [45] studied the effect of PEO time of coating on Ti-6Al-4V alloy under constant voltage conditions on corrosion and abrasion properties in the existence of phosphate-silicate electrolyte. They realized that shorter time was good for corrosion properties and longer times for abrasive properties of coatings. However, there is little data on the effect of coating time in the existence of electrolytes containing nanoparticles for coatings that were formed on Ti-6Al-4V alloy. The purpose of this research was to run zirconium titanate ceramic coating having zirconia nanoparticles and to find the relationship between different stages of coating with microstructure and corrosion properties in Hank's physiological solution and to investigate the fuzzy composition of PEO process coatings.

2. Experimental procedure

2.1. PEO procedure

In this research, Ti-6Al-4V alloy was utilized as the substrate for PEO procedure, which chemical composition was shown in Table 1. In order to make the substrates ready, the specimens were firstly polished using 60 to 800 papers of grit grinding. Then, the specimens were washed using distilled water. Afterwards, they were dried through blasting of cold air.

To do the PEO treatment, the specimens were immersed inside the solutions that have distilled water, 12 g/L $Na_3PO_4.12H_2O$ (provided by Merk co.) and 3 g/L ZrO_2 nanoparticles (with the average size of 40 nm). The ultrasonic treatment was utilized in order to ensure the steady nanoparticles dispersion in solutions for 1 h.

Table 1. Chemical composition of the Ti-6Al-4V substrate

Element	Ti	Al	V	Fe	C	O	N	H
Wt%	89.94	5.8	4.13	0.05	0.01	0.06	0.009	0.001

The power supply of DC pulsed having the highest voltage of 700 V was applied in order to carry out PEO procedure. Then after, the container of stainless steel and the supplied specimens were respectively corresponded to the positive (anode) poles and negative (cathode) of the tool. The samples fabricated in different processing time consisting 5, 10 and 15 min were labeled as T5, T10 and T15 orderly. In all tests, the duty cycle parameters, current density and frequency were taken up at 50 %, 1000 Hz and 2 A/dm^2, respectively. The changes in voltage as a function of procedure time were recorded in order to study the happenings within the coating procedures. After the procedures, being immersed in the distilled water for 10 min, the specimens were dried using cold air blasting.

2.2. Surface characterization

Patterns of XRD were acquired by diffractometer of Philips PW1730 in order to assess the coatings phase composition. The coatings XRD measurements were done by Cu Kα radiation in addition to 0.05º step scan in a range of 2θ between 10º and 80º. The images of scanning electron microscopy (SEM) were acquired in order to investigate the cross-section of the specimens and the surface microstructure. The measurement was carried out using a microscope of JEOL JSM-840A. Besides, the thickness calculation and coatings porosity size was done using software of MIP. Distinct tests were done at various zones and at last, the mean values were reported for each specimen. In addition, a more precise investigation on coatings was carried out by the field emission SEM TESCAN Mira3 XMU and also an energy dispersive spectrometer (EDS). The tester of surface roughness (RT2200 model) was utilized in order to specify the specimens surface roughness. The measurements of surface roughness were performed at three distinct zones and finally, the mean value was presented.

2.3. The electrochemical behavior of coatings

The electrochemical impedance spectroscopy (EIS) and potentiodynamic polarization

tests were performed in Hank's physiological solution. Table 2 presents the chemical composition of utilized Hank's electrolyte in this study [36]. The corrosion measurements were carried out by appliance of μautolab having a three-electrode method composing of an Ag/AgCl reference electrode, platinum counter electrode and a coated specimen as the working electrode. The working electrodes were immersed in the electrolyte for 120 min in order to acquire a steady condition before the tests. Then, the EIS measurements were performed in the frequency range of 100 kHz to 10 mHz via the wavelength range of ±10 mV. Furthermore, the polarization investigations were also carried out having the potential range of -0.250 V under the open circuit potential to 2.0 V having the 1 mV/s scan rate. The tests were repeatedly done for a couple of times at least in order to assure the results precision. NOVA 1.7 software was utilized to analyze the results of corrosion measurement.

Table 2. Chemical composition of Hank's solution

Chemical Reagent	Amount (g/l)
NaCl	8
KCl	0.4
$CaCl_2$	0.14
$NaHCO_3$	0.35
$NaH_2PO_4{\cdot}2H_2O$	0.06
KH_2PO_4	0.06
$Mg_2SO_4{\cdot}7H_2O$	0.06
$MgCl_2.6H_2O$	0.1
$C_6H_{12}O_2.H_2O$	1

3. RESULT AND DISCUSSION

3.1. Voltage-time diagram

When using a constant current mode in the PEO procedure, the voltage behavior is recorded than the coverage time. Fig. 1 shows the voltage-time diagram for the ceramic coating formed on the Ti-6Al-4V alloy at a constant current density of 2 A/dm^2 and a duration of 15 minutes. Based on this diagram, the coating is formed in 4 different steps in the presence of alkaline electrolyte for 15 minutes. At first, the PEO procedure begins with anodic oxidation that is also known as conventional anodizing. Under these conditions, the voltage increases linearly at a high rate (9.16 V/s) and reaches 265 V in 28 seconds due to the application of current to the sample. What occurs on the surface of the sample includes the substrate dissolution, the penetration of O^{2-} ions into the interface of oxide/ metal, the severe evolution of the gas and finally the formation of a barrier layer with a columnar structure perpendicular to the surface of substrate [46].

$$Ti \rightarrow Ti^{4+} + 4e^- \quad (1)$$

$$H_2O \rightarrow OH^- + H^+ \quad (2)$$

$$2\,OH^- \rightarrow O^{2-} + \ H_2O \quad (3)$$

$$2\,H_2O \rightarrow O_2 + 4H^+ + 4e^- \quad (4)$$

$$Ti^{4+} + 2O^{2-} \rightarrow TiO_2 \quad (5)$$

$$Ti^{4+} + \ 2\,H_2O \rightarrow TiO_2 + 4H^+ \quad (6)$$

$$Ti^{4+} + 2OH^- + \ 2\,H_2O \rightarrow TiO_2 \ + 2\ H_3O^+ \quad (7)$$

The following reactions describe what happens at this stage [46,47]. When the voltage reaches the breakdown potential (265 V), the second stage of the coating procedure starts. Very small sparks appear due to the occurrence of dielectric failure by starting the second step on the surface of the anode [44]. The second phase occurred between 18 and 300 seconds after the coating process and the voltage change rate reached 1.13 V/s. Introducing the third step, the size of the sparks increases and their number decreases. This step is in the range of 300 to 600 seconds from the procedure and the rate of voltage change is 0.1 V/s. In the fourth step of the procedure, the voltage change rate got zero, indicating a steady discharge on the surface of the growing oxide coating. In the fourth step, the sparks get large arcs having long life and high intensity.

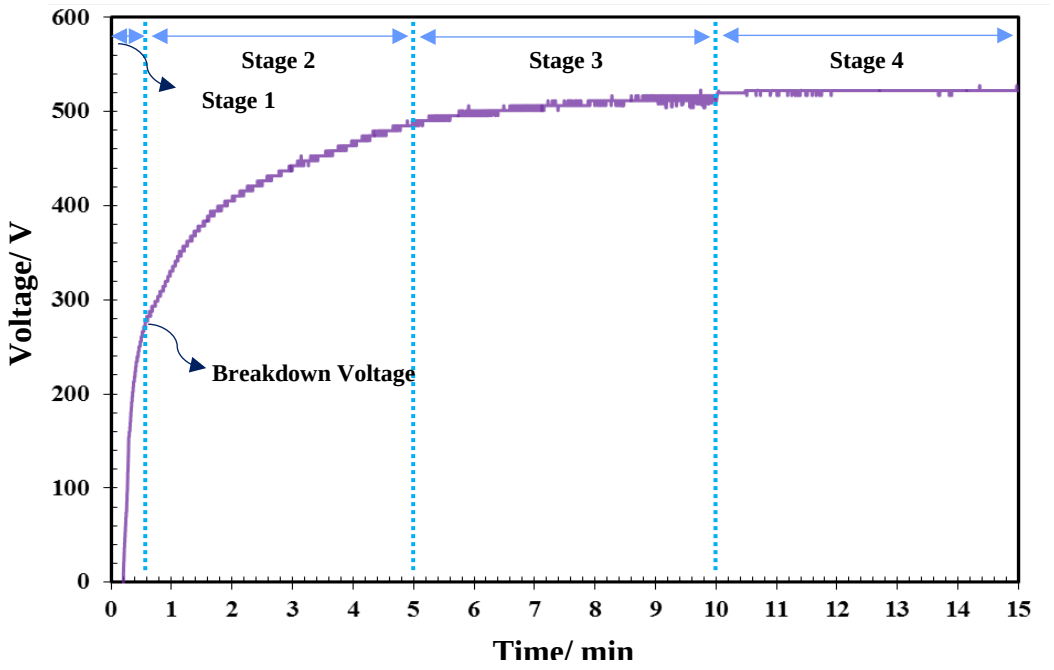

Fig. 1. Voltage-time diagram to produce coating on the Ti-6Al-4V alloy for 15 minutes

In the PEO procedure, the whole current passing through the oxide layer includes ionic and electron currents. In the first step, only the ionic current passes through the coating. Whereas in the next steps, the sum of ionic and electron currents passes through the growing coating by the occurrence of the dielectric failure phenomenon. Electron current is accompanied by electron avalanches and is made by the evolution of oxygen. When electron and ionic currents pass through the coating, a lower voltage is required to keep the current density constant (2 A/cm^2). Consequently, the rate of voltage change decreases through the time [48].

3.2. Surface analysis

The main characteristic of the coating created by the PEO procedure after the dielectric failure is the cavities that arises from the exit of the plasma bubbles from the discharge channels and their explosion on the surface of coating [49]. According to Fig. 2 (a-c) and based on the response of voltage-time, some cavities are seen on the surface of all coatings at the end of the second, third and fourth steps of the coating but the number and size of cavities produced on the samples surface are different at different steps.

Fig. 3 shows a columnar diagram correlated with percentage values and size of the porosities at various times of coating. As can be seen in Fig. 3, the pores size rises with the coating procedure time. The porosity size of the T10 and T15 specimens are about 2 and 4 times more than that of the T5 specimens, respectively. This might be owing to an increase in coating time and thickening the coating that reduces the amount of available sites for micro-discharge formation. Under these conditions, the anodic current requires higher energy to pass through a thicker coating and reach the substrate. Thus, the number of micro-discharges decreases, but their average size increases. As can be seen in Fig. 3, the T10 and T15 specimens have the least and most porosity percentage, respectively. The T15 has a higher percentage of porosity than other specimens because of its larger porosity. Although the T5 has smaller porosities than the T10, it has more porosities than the T10. Thus, the T10 specimen has the least porosity percentage. Fig. 2 (d-f) indicates the cross-sectional images of the coatings created at 5, 10, and 15 minutes. A good adhesion between all the coatings and the substrate is observed. As can be seen, ceramic coatings made by the PEO procedure will increase. Within 5 minutes, a coating with an average thickness of 5.2 μm was obtained. Furthermore, the average final thickness for coatings created over time 10 and 15 minutes, respectively, are equal to 10.7 and 12.6 μm, respectively by rising time of coating. This increase in thickness is due to the increase in ignition voltage at higher times. High ignition voltage leads to higher energy sparks and as a result the production of molten material. These molten materials can much easily exit the discharge channel and precipitate on the surface at high temperatures, producing a thicker oxide coating [50]. The thickness of the T10 specimen has been about doubled in comparison to the T5, while the thickness of the T15 is about 0.81

time than that of the T10. the coating growth rate of T10, T5 and T 15 specimens are 1.04 , 1.07 and 0.84 µm/ min respectively that indicate as the coating time increases from 10 to 15 minutes, the growth rate of the coating decreases that can be due to a decline in the voltage change rate than the coating time.

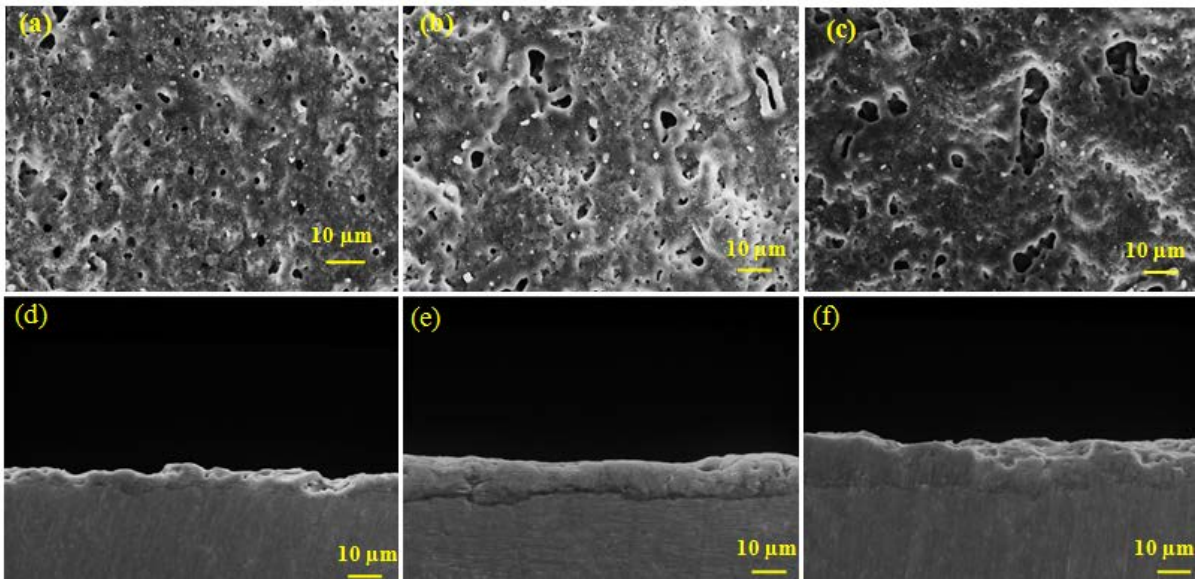

Fig. 2. SEM images of surface and cross-section of coatings surface obtained from PEO procedures: (a, d) T5, (b, e) T10, and (c, f) T15

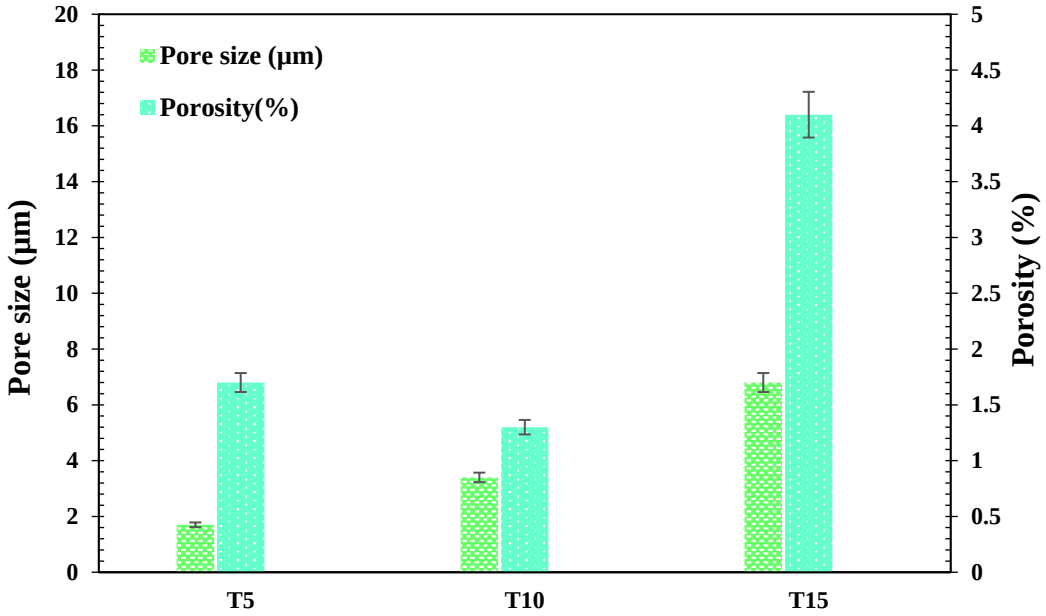

Fig. 3. Columnar diagram of the size and percentage of porosity of the coatings produced at distinct times

3.3. Roughness of coatings

Fig. 4 shows the obtained results of the roughness for the surface of the coatings formed at various times of coating and substrate. As can be seen, the values of Ra and Rz of the coatings have improved in comparison to the substrate.

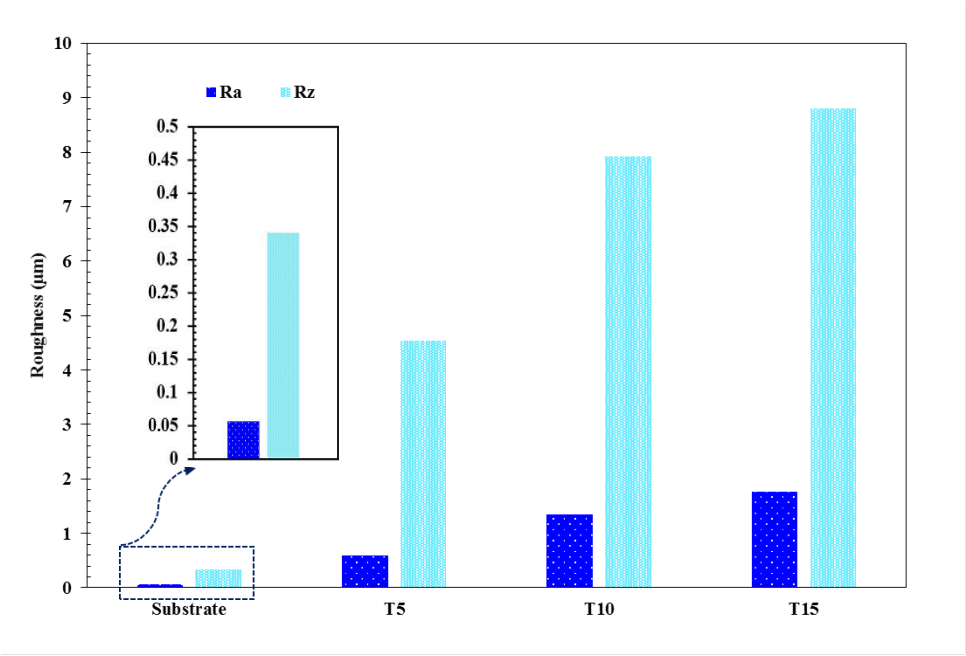

Fig. 4. Columnar diagram for the roughness of the coatings produced at different times and the substrate

In addition, it is observed that the roughness values of Ra and Rz increase by raising the coating time from 5 to 15 minutes. If the values of roughness are less and more than 1 µm, it is known as smooth and rough surface, respectively [51]. A rougher surface lets more adhesion and an increase in osteoblasts than smooth surface [15]. So, it can be concluded that the specimens created at the end of the third and fourth steps of coating can be more useful for bone tissue growth.

3.4. Phase composition and elemental study of coatings

The XRD pattern for the created specimens at different times is shown in Fig. 5. All coatings contain $ZrTiO_4$ and ZrO_2 phases and there is no peak of titanium oxide. This means that some ZrO_2 nanoparticles participated in the coating formation without forming a new phase and some other nanoparticles melted under the effect of high discharge energy and then reacted with molten TiO_2 to form a new phase such as $ZrTiO_4$. Shin et al. [52] and Gowtham et al. [53] also reported some reactive incorporation of zirconia particles into the oxide coating created on titanium and its alloys and the formation of the $ZrTiO_4$ phase.

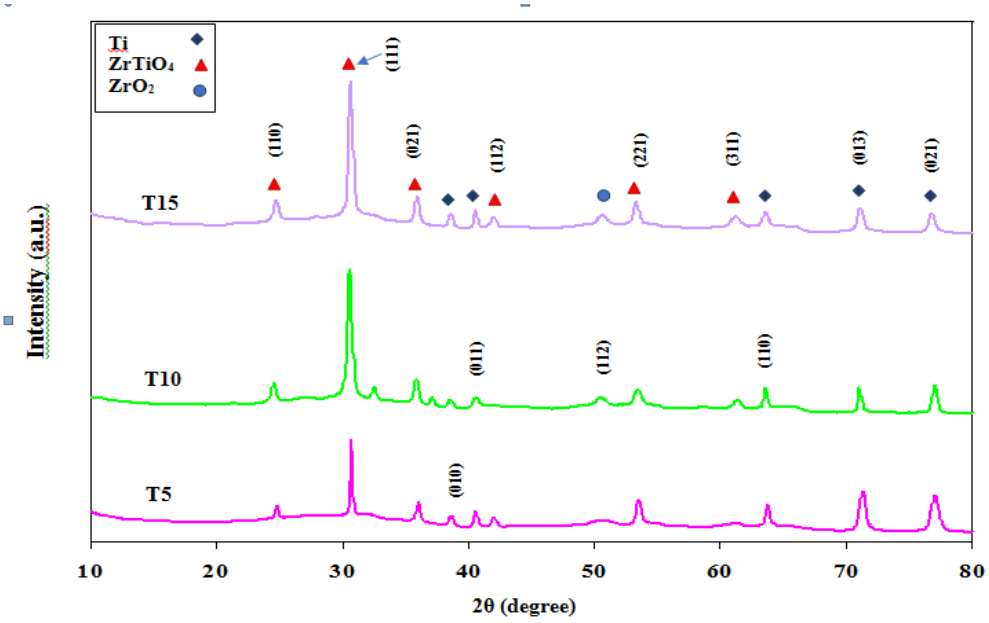

Fig. 5. XRD pattern for coatings produced at different times of coating

In addition, the Ti peak is also observed due to its low thickness and porous nature of the coatings. As the coating time increases, the intensity of the $ZrTiO_4$ and ZrO_2 peaks increases, while the intensity of the Ti peak decreases. The reason of the decrease in the peak intensity is the increase in coating thickness from 5.2 to 12.6 µm. In the third and fourth steps, the ignition coating process occurs with greater intensity, so the temperature of the discharge channels gets higher. This can facilitate the conditions for chemical, electrochemical, and chemical-thermal reactions and this may be the reason of the increase in the $ZrTiO_4$ phase value with increasing coating time. In addition, more electrolyte components are involved in the coating as the coating time increases. Consequently, it can be concluded that more nanoparticles enter the coating.

Figs. 6 and 7 show the distribution of the main component elements on the surface and the cross-section of the produced coating within 10 minutes, respectively. The main components of ceramic coating contain Zr, P, Ti and O. The sources of Zr and P elements are the electrolytes containing sodium phosphate and zirconia nanoparticles, respectively and the source of the Ti element is the substrate. Fig. 6 exhibits that Zr has been steadily distributed on the surface. The reason for the steady distribution of Zr may be ascribed to its reactive penetration into the coating. As the XRD results indicated, the main constituent phase is the $ZrTiO_4$ oxide coating. For this reason, Zr can be expected to be present almost steady on the surface. In addition, it is observed that the element P is steadily present on the surface. The presence of P in the coating can improve the bioactivity of the coating [54]. In Fig. 7, the distribution of O in the coating in comparison to the substrate is highly increased due to the formation of the oxide coating. In addition, it is seen that the electrolyte components (Zr and P) are distributed almost steadily in the cross-section of the coating. Some researchers [55,56] have identified the outer layer of the coating as a trap for nanoparticles,

while the Zr signals have been identified almost steadily throughout the coating. This indicates that zirconia nanoparticles having a diameter of 40 nm can deeply penetrate into the coating.

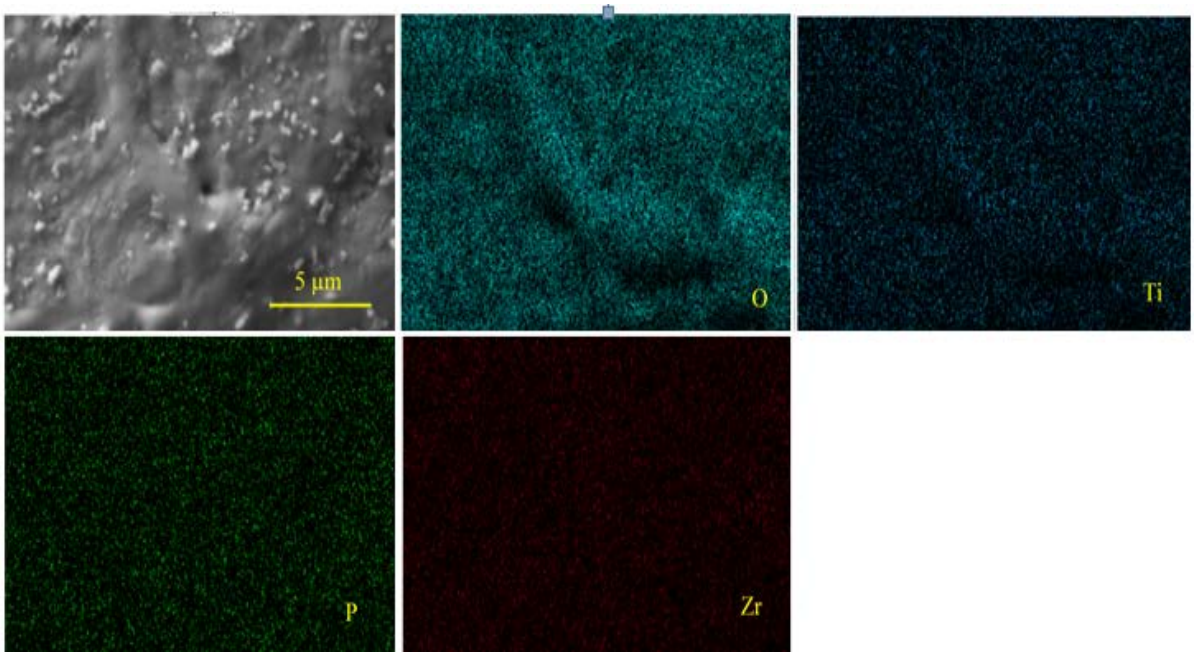

Fig. 6. Distribution map of the main component elements of the T10 sample surface

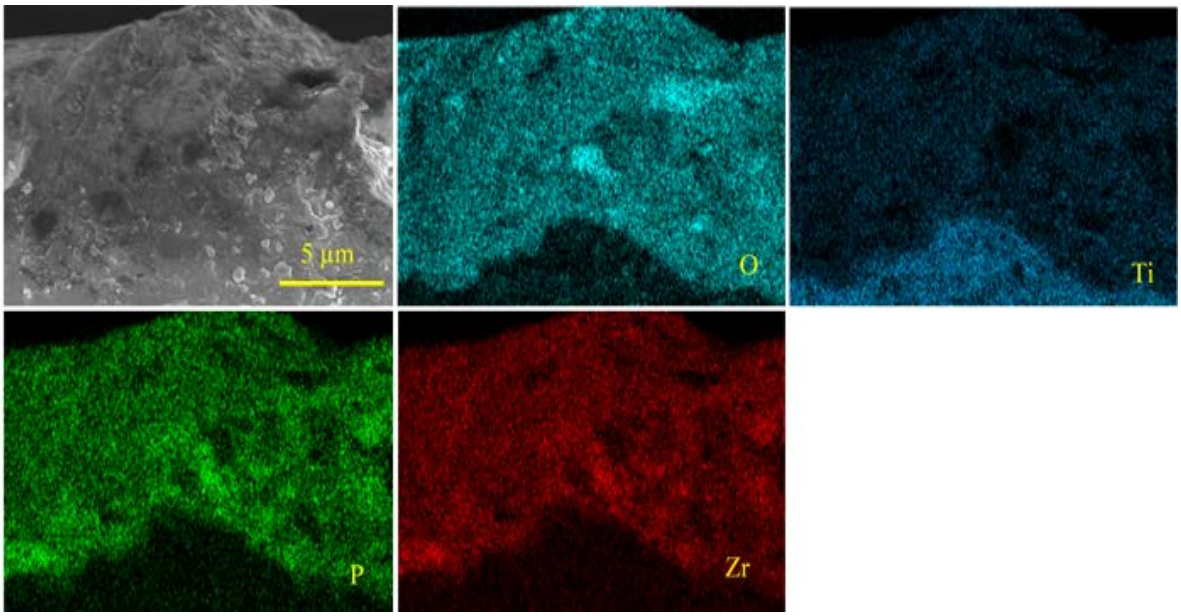

Fig. 7. Distribution map of the main component elements from the cross-section of the T10 sample

3.5. Studying the corrosion behavior of coatings

The spectroscopy test of the electrochemical impedance was used in order to obtain extensive information about the electrochemical behavior of the coatings created in the different steps of the coating. Fig. 8 shows the obtained Bode and Nyquist curves from the EIS test for T5, T10 and T15 specimens. Nyquist plots of coated specimens at different times (Fig. 8(a)) have the same shape in the presence of phosphate electrolytes containing zirconia nanoparticles and all of them are composed of two capacitive loops.

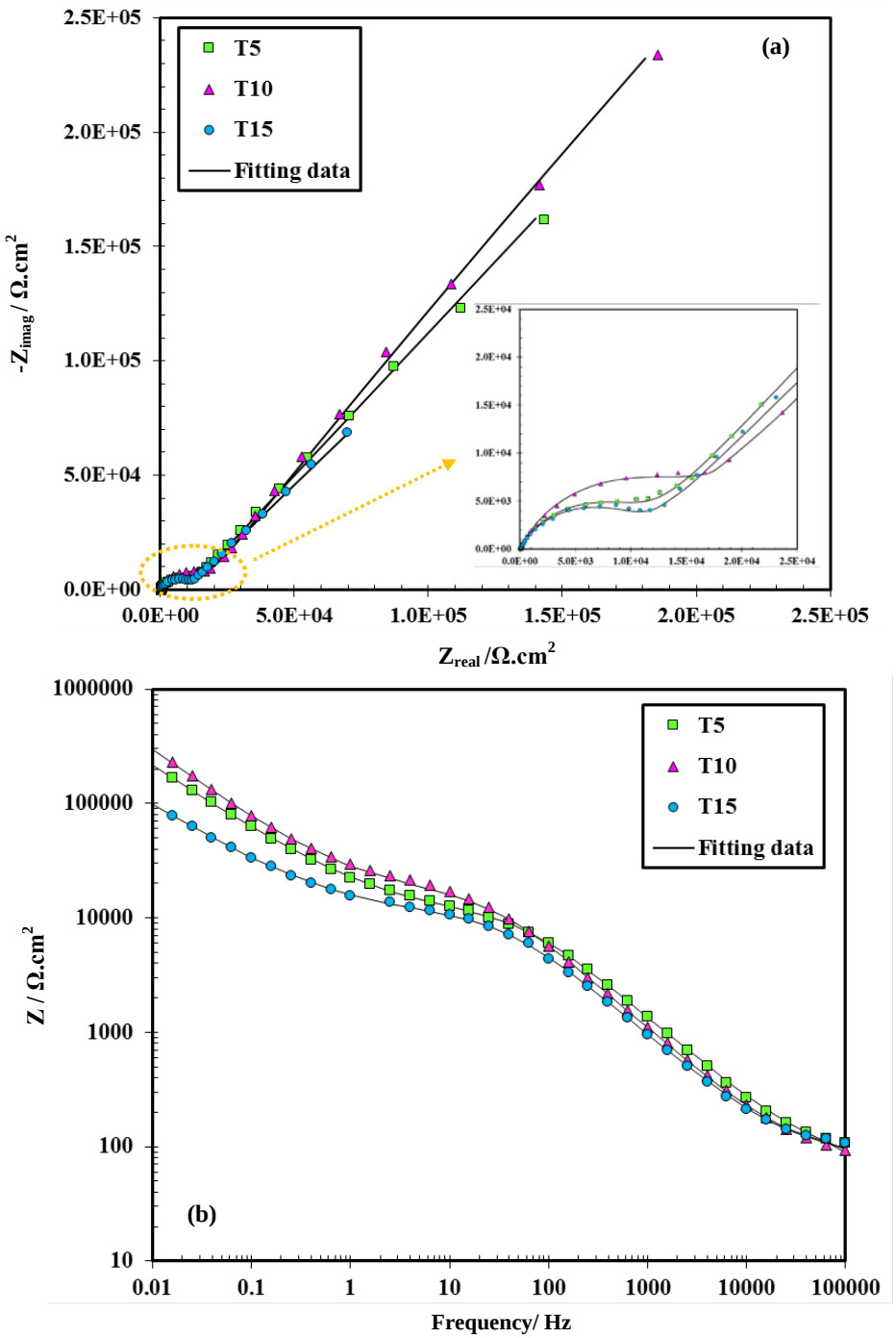

Fig. 8. (a) Nyquist and (b) Bode plots of the coated samples at distinct times of coating

The smaller half-loop that appears at high frequencies is related to the corrosion resistance of the porous outer layer and the larger half-loop is related to the dense inner layer and appears at lower frequencies. Comparing the diameter of the curve loops in the Nyquist plot, it can be observed that the T10 specimen has the highest loop diameter and as a result the highest corrosion resistance. It is seen in the Bode curves (Fig. 8(b)) that at low frequencies, the impedance value (Z) for the T15, T5 and T10 samples increase, respectively and an increase in the impedance value indicate a rise in corrosion resistance. Consequently, the T10 specimen presents the best corrosion behavior. To model the corrosion behavior of the coatings, the equivalent electrical circuit (EEC) of Fig. 9 was used. In this EEC, resistance of solution between coating surface and the reference electrode, electrical resistance of the inner and outer layers are labeled as R_s, R_i and R_o respectively. Moreover, the constant phase element (CPE) of the inner and outer layer are indicated by CPE_i and CPE_o [57–62]. The values of the obtained elements from the modeling the corrosion behavior of the coatings are listed in Table 3. Ignoring the different times of coating, it should be considered that the resistance of the solution is almost the same for all three samples whereas the strength of the inner layer of the coatings is much bigger than the resistance of outer layer due to having fewer defects and denser structure. The created sample within 10 minutes has the most resistance of the inner layer (3 $M\Omega.cm^2$) and the outer layer (18.28 $k\Omega.cm^2$) and as a result the best corrosion behavior. The produced sample within 15 minutes with the least resistance of the inner layer (0.84 $M\Omega.cm^2$) and the outer layer (11.60 $k\Omega.cm^2$), has the most unpleasant behavior among the coatings.

Table 3. Extracted data from the proposed equivalent circuit

Sample	R_s ($\Omega.cm^2$)	n_o	Q_o ($\mu F.cm^{-2}$)	R_o ($k\Omega.cm^2$)	n_i	Q_i ($\mu F.cm^{-2}$)	R_i ($M\Omega.cm^2$)
T5	74.00	0.766	1.27	12.02	0.619	24.75	2.04
T10	74.4.	0.774	1.24	18.28	0.646	19.80	3.00
T15	75.20	0.747	1.67	11.60	0.598	55.00	0.84

Fig.10 illustrates a potentiodynamic polarization plot in Hank's physiological solution for the produced coatings at distinct coating times. Similar electrochemical behavior is observed for coatings. As the coating time increased from 5 to 10 minutes, the potentiodynamic polarization curve shifted to a more noble potential and less corrosion current density, while the corrosion potential and current density declined and increased, respectively by increasing time of coating to 15 minutes. The extracted data from the polarization plots is presented in Table 4. In this table, the corrosion resistance of the samples

is calculated using the Stern-Gray equation [63]:

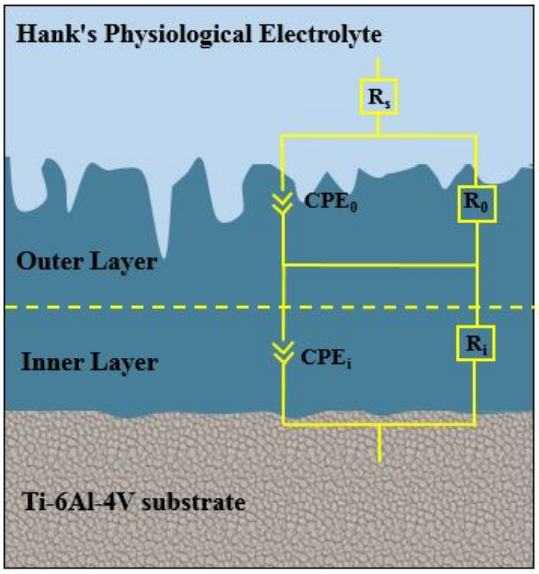

Fig. 9. The proposed EEC to model the corrosion behavior of coatings

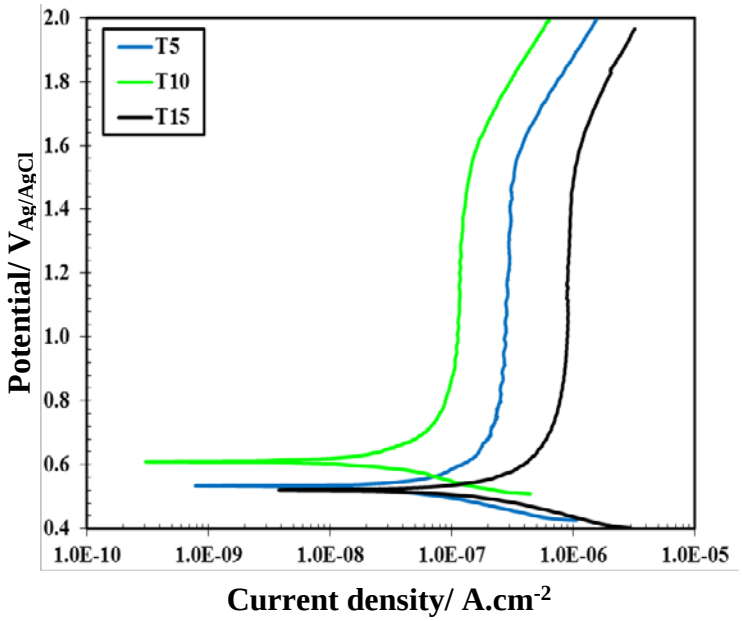

Fig. 10. Potentiodynamic polarization curves for coated samples at different times of coating

$$R_p = \frac{\beta_a \beta_c}{2.3(\beta_a + \beta_c) i_{corr}} \quad (8)$$

In this equation, β_a and β_c are called anodic and cathodic slope, respectively and R_p is polarization resistance. According to Table 4, the T10 sample has the highest corrosion potential, showing a lower thermodynamic tendency for corrosion than the T5 and T15. In

addition, the T10 sample has the least corrosion current density (18.50 nA/cm^2) and so the highest polarization resistance (0.602 MΩ.cm^2). The lowest slope of the anodic branch is related to the T10 sample showing that the anodic reaction occurs less rapidly on the surface of the T10 sample that slows down the corrosion rate of the T10 sample in comparison to the T5 and T15 specimens.

Table 4. Electrochemical data obtained from the potentiodynamic polarization curve for samples coated at different times of coating

Sample	E_{corr} (mV)	i_{corr} (nA.cm^{-2})	β_a (mV/dec)	β_c (mV/dec)	R_p (MΩ.cm^2)
T5	531	25.67	48.99	74.65	0.499
T10	611	18.50	44.03	61.62	0.602
T15	520	75.17	60.00	79.19	0.197

Comparing the corrosion resistance of the coatings and the percentage of porosity reported in Fig. 3, a direct relation between these two parameters is found. As can be seen in Fig. 3, the T10 and T15 specimens have the lowest and highest porosity percentages, respectively causing them to have the most and least polarization resistance. The T15 specimen has the lowest polarization resistance (0.197 MΩ.cm^2) among the specimens, despite having the highest thickness (12.1 µm). This indicates that the thickness of the coating does not have a significant effect on improving the corrosion resistance of the coatings and the porosity percentage of the coatings determines the corrosion properties of the coatings. Indeed, porosities that are one of the most important defects of PEO coatings plays a major role in specifying the various coating properties, particularly in corrosion resistance since corrosive solution can penetrate the coating through the porosities and eventually attain the substrate through ruining the coating. Thus, the T10 specimen is more appropriate against the penetration of corrosive solution due to having a lower porosity percentage.

4. CONCLUSION

In this study, the effect of different coating times on the microstructure and corrosion behavior of the coatings formed on Ti-6Al-4V alloy that was treated in the same coating bath containing zirconia nanoparticles was investigated. It was obviously observed that SEM images of coated samples exhibited that rising the coating time from 5 to 15 minutes resulted in an increase in coating thickness from 5.2 to 12.6 µm and an increase in the size of porosity from 1.7 to 6.8 µm. Furthermore, the porosity percentage of the samples increased in 10, 5 and 15 minutes for the coatings, respectively. On the other hand, the PEO procedure led to an

increase in the substrate roughness and the coating roughness increased from 0.65 μm to 1.86 μm by rising coating time from 5 to 15 min. Moreover, the results of the XRD pattern of the coatings showed no change in the chemical composition of the coatings and just made intensity in the peaks related to ZrO_2 and $ZrTiO_4$ by increasing coating time. Finally, potentiodynamic polarization tests showed that increasing the coating time from 5 to 10 minutes led to a decrease in corrosion current density and increasing the time further to 15 minutes raised the corrosion current density; so, the coating produced within 10 minutes had the lowest corrosion density (18.50 nA/cm^2) and consequently the best corrosion resistance (0.602 $M\Omega.cm^2$).

REFERENCES

[1] Q. Chen, and G.A. Thouas, Mater. Sci. Eng. R 87 (2015) 1.

[2] E. Matykina, R. Arrabal, B. Mingo, M. Mohedano, A. Pardo, and M.C. Merino, Surf. Coat. Technol. 307 (2016) 1255.

[3] A. Fattah-alhosseini, O. Imantalab, and G. Ansari, Mater. Sci. Eng. C 71 (2017) 827.

[4] I.J. Hwang, and H.C. Choe, Appl. Surf. Sci. 432 (2018) 337.

[5] K. Wang, Mater. Sci. Eng. A 213 (1996) 134.

[6] G. Ansari, and A. Fattah-alhosseini, Mater. Sci. Eng. C 75 (2017) 64.

[7] M. Geetha, A.K. Singh, R. Asokamani, and A.K. Gogia, Prog. Mater. Sci. 54 (2009) 397.

[8] R. Khanna, T. Kokubo, T. Matsushita, Y. Nomura, N. Nose, Y. Oomori, T. Yoshida, K. Wakita, and H. Takadama, Mater. Sci. Eng. C 55 (2015) 393.

[9] M. Khorasanian, A. Dehghan, M.H. Shariat, M.E. Bahrololoom, and S. Javadpour, Surf. Coat. Technol. 206 (2011) 1495.

[10] S.J. Li, R. Yang, S. Li, Y.L. Hao, Y.Y. Cui, M. Niinomi, and Z.X. Guo, Wear 257 (2004) 869.

[11] A. Fattah-alhosseini, A.R. Ansari, Y. Mazaheri, and M.K. Keshavarz, Mater. Sci. Eng. C 71 (2017) 771.

[12] K. Subramani, R.T. Mathew, P. Pachauri, Titanium surface modification techniques for dental implants-From microscale to nanoscale, Second Edi, Elsevier Inc., 2018.

[13] A. Fattah-alhosseini, M.K. Keshavarz, M. Molaei, and S.O. Gashti, Metall. Mater. Trans. A 49 (2018) 4966.

[14] J. Yu, and H. Choe, Appl. Surf. Sci. 432 (2018) 294.

[15] Y. Han, S.H. Hong, and K. Xu, Surf. Coat. Technol. 168 (2003) 249.

[16] C.A.H. Laurindo, R.D. Torres, S.A. Mali, J.L. Gilbert, and P. Soares, Mater. Sci. Eng. C 37 (2014) 223.

[17] S. Stojadinović, R. Vasilić, M. Petković, B. Kasalica, I. Belča, A. Žekić, and L. Zeković, Appl. Surf. Sci. 265 (2013) 226.

[18] M. Molaei, A. Fattah-Alhosseini, and S.O. Gashti, Metall. Mater. Trans. A 49 (2018) 368.

[19] M. Molaei, A. Fattah-alhosseini, and M.K. Keshavarz, J. Asian Ceram. Soc. 7 (2019) 247.

[20] M. Roknian, A. Fattah-alhosseini, and S.O. Gashti, J. Mater. Eng. Perform. 27 (2018) 1343.

[21] T.S.N. Sankara Narayanan, I.S. Park, and M.H. Lee, Prog. Mater. Sci. 60 (2014) 1.

[22] A. Fattah-alhosseini, K. Babaei, and M. Molaei, Surf. Interfaces 18 (2020) 100441.

[23] T.W. Clyne, and S.C. Troughton, Int. Mater. Rev. 64 (2019) 127.

[24] R. Chaharmahali, A. Fattah-alhosseini, and H. Esfahani, J. Asian Ceram. Soc. 8 (2020) 39.

[25] A. Fattah-alhosseini, and M.S. Joni, J. Mater. Eng. Perform. 24 (2015) 3444.

[26] Z. Masoomi Loghman, A. Fattah-alhosseini, and S.O. Gashti, Anal. Bioanal. Electrochem. 10 (2018) 1247.

[27] Z. Masoomi Loghman, A. Fattah-Alhosseini, and S.O. Gashti, Anal. Bioanal. Electrochem. 11 (2019) 1020.

[28] A. Fattah-alhosseini, M. Molaei, N. Attarzadeh, K. Babaei, and F.R. Attarzadeh, Ceram. Int. (2020) https://doi.org/10.1016/j.ceramint.2020.05.206.

[29] M. Vakili-Azghandi, and A. Fattah-alhosseini, Metall. Mater. Trans. A 48 (2017) 4681.

[30] R. Chaharmahali, M. Shadabi, K. Babaei, S.O. Gashti, and A. Fattah-alhosseini, Anal. Bioanal. Electrochem. 11 (2019) 38.

[31] A. Fattah-alhosseini, M. Molaei, and K. Babaei, Anal. Bioanal. Electrochem. 12 (2020) 517.

[32] X. Ma, C. Blawert, D. Höche, M.L. Zheludkevich, and K.U. Kainer, Appl. Surf. Sci. 388 (2016) 304.

[33] X. Lu, M. Mohedano, C. Blawert, E. Matykina, R. Arrabal, K.U. Kainer, and M.L. Zheludkevich, Surf. Coat. Technol. 307 (2016) 1165.

[34] X. Lu, C. Blawert, M.L. Zheludkevich, and K.U. Kainer, Corros. Sci. 101 (2015) 201.

[35] X. Lu, C. Blawert, Y. Huang, H. Ovri, M.L. Zheludkevich, and K.U. Kainer, Electrochim. Acta 187 (2016) 20.

[36] E. Nikoomanzari, A. Fattah-alhosseini, M.R. Pajohi Alamoti, and M.K. Keshavarz, Ceram. Int. 46 (2020) 13114.

[37] J. Macan, A. Gajović, and H. Ivanković, J. Eur. Ceram. Soc. 29 (2009) 691.

[38] I.C. Cosentino, E.N.S. Muccillo, and R. Muccillo, Sensors Actuators B Chem. 96 (2003) 677.

[39] S. Minagar, Y. Li, C.C. Berndt, and C. Wen, Acta Biomater. 12 (2015) 281.

[40] E. Salahinejad, M.J.J. Hadianfard, D.D.D. MacDonald, I. Karimi, D. Vashaee, and L. Tayebi, Ceram. Int. 38 (2012) 6145.

[41] H. Li, Y. Sun, and J. Zhang, Appl. Surf. Sci. 342 (2015) 183.
[42] S. Stojadinović, N. Radić, R. Vasilić, M. Petković, P. Stefanov, L. Zeković, and B. Grbić, Appl. Catal. B Environ. 126 (2012) 334.
[43] E. Santos, G.B. de Souza, F.C. Serbena, H.L. Santos, G.G. de Lima, E.M. Szesz, C.M. Lepienski, and N.K. Kuromoto, Surf. Coat. Technol. 309 (2017) 203.
[44] V. Dehnavi, D.W. Shoesmith, B.L. Luan, M. Yari, X.Y. Liu, and S. Rohani, Mater. Chem. Phys. 161 (2015) 49.
[45] Y. Cheng, X. Wu, Z. Xue, E. Matykina, P. Skeldon, and G.E. Thompson, Surf. Coat. Technol. 217 (2013) 129.
[46] S. Sarbishei, M.A. Faghihi Sani, and M.R. Mohammadi, Ceram. Int. 42 (2016) 8789.
[47] A.L. Yerokhin, A. Leyland, and A. Matthews, Appl. Surf. Sci. 200 (2002) 172.
[48] L.O. Snizhko, A.L. Yerokhin, A. Pilkington, N.L. Gurevina, and D.O. Misnyankin, Electrochim. Acta 49 (2004) 2085.
[49] E. Matykina, A. Berkani, P. Skeldon, and G.E. Thompson, Electrochim. Acta 53 (2007) 1987.
[50] A.L. Yerokhin, L.O. Snizhko, N.L. Gurevina, A. Leyland, A. Pilkington, and A. Matthews, J. Phys. D: Appl. Phys. 36 (2003) 2110.
[51] L. Xu, C. Wu, X. Lei, K. Zhang, C. Liu, J. Ding, and X. Shi, Surf. Coat. Technol. 342 (2018) 12.
[52] K.R. Shin, Y.G. Ko, and D.H. Shin, Mater. Lett. 64 (2010) 2714.
[53] S. Gowthaw, S. Hariprasad, T. Arunnellaiappan, and N. Rameshbabu, Surf. Coat. Technol. 313 (2017) 263.
[54] R.F. Zhang, L.P. Qiao, B. Qu, S.F. Zhang, W.H. Chang, and J.H. Xiang, Mater. Lett. 153 (2015) 77.
[55] M. Roknian, A. Fattah-alhosseini, S.O. Gashti, and M.K. Keshavarz, J. Alloys Compd. 740 (2018) 330.
[56] A. Seyfoori, S. Mirdamadi, Z.S. Seyedraoufi, A. Khavandi, and M. Aliofkhazraei, Mater. Chem. Phys. 142 (2013) 87.
[57] R. Chaharmahali, K. Babaei, and A. Fattah-alhosseini, Anal. Bioanal. Electrochem. 11 (2019) 703.
[58] A. Fattah-alhosseini, M. Vakili-Azghandi, and M.K. Keshavarz, Acta Metall. Sin. (English Lett. 29 (2016) 274.
[59] M. Sabaghi Joni, and A. Fattah-alhosseini, J. Alloys Compd. 661 (2016) 237.
[60] A. Keyvani, M. Zamani, A. Fattah-alhosseini, S.H. Nourbakhsh, and M. Bahamirian, Mater. Res. Express. 5 (2018) 086510.
[61] A. Khodabandeloie, and A. Fattah-alhosseini, Anal. Bioanal. Electrochem. 10 (2018) 1574.

[62] M. Vakili-Azghandi, A. Fattah-alhosseini, and M.K. Keshavarz, J. Mater. Eng. Perform. 25 (2016) 5302.
[63] G.H. Lv, H. Chen, L. Li, E.W. Niu, H. Pang, B. Zou, and S.Z. Yang, Curr. Appl. Phys. 9 (2009) 126.